Temperature dependent state-of-charge estimation of lithium ion battery using dual spherical unscented Kalman filter

Aung, Htet; Low, Kay Soon

2015

Aung, H., & Low, K. S. (2015). Temperature dependent state-of-charge estimation of lithium ion battery using dual spherical unscented Kalman filter. IET Power Electronics, 8(10), 2026-2033.

https://hdl.handle.net/10356/81592

https://doi.org/10.1049/iet-pel.2014.0863

Research Article

Temperature dependent state-of-charge estimation of lithium ion battery using dual spherical unscented Kalman filter

ISSN 1755-4535
Received on 8th November 2014
Revised on 6th April 2015
Accepted on 28th April 2015
doi: 10.1049/iet-pel.2014.0863
www.ietdl.org

Htet Aung ✉, *Kay Soon Low*

School of Electrical and Electronic Engineering, Satellite Research Center (SaRC), Nanyang Technological University, Block S2, S2.2-B3-06, 50 Nanyang Avenue, Singapore 639798, Singapore

✉ *E-mail: aung0083@e.ntu.edu.sg*

Abstract: Accurate and reliable state-of-charge (SOC) estimation is an important task for battery management system in a satellite. Ambient temperature is one of the significant factors that affect SOC estimation. Since satellite operates at different temperatures throughout the orbit, it must be taken care of accordingly to safeguard the battery performance and reliability. Moreover, SOC estimation depends on battery model accuracy as well. The battery parameters are affected by temperature, SOC, charging and discharging rates. Hence, the parameters need to be updated accordingly to improve the battery model and the SOC estimation accuracy. In this study, a SOC estimation method and online parameter updating using a dual square root unscented Kalman filter based on unit spherical unscented transform is proposed. The proposed method has been validated experimentally and the results are compared with extended Kalman filter and unscented Kalman filter based on unit spherical unscented transform. Experimental results have shown that the proposed method has better performance in terms of lower root mean square error and absolute maximum error.

1 Introduction

Lithium ion battery has become increasingly popular in satellite power applications because of its high energy density and weight ratio. Unlike other applications, servicing of hardware is infeasible once the satellite is launched. Consequently, the safety and reliability of the battery is of paramount important in satellite applications. Over charging or discharging can cause irreversible damage to the battery which would fail the satellite mission. Proper control in terms of reliable and accurate state-of-charge (SOC) estimation is necessary to safeguard the battery performance and operation of a satellite. SOC indicates the present available charge to its rated nominal charge capacity. It is used in mission planning of a satellite. However, SOC cannot be measured directly and it is estimated from measurable quantity such as battery's current and voltage. The operational requirement at different temperatures for satellite applications is one vital factor that affects the accuracy of SOC estimation and battery parameters.

Many SOC estimation methods have been presented [1–16]. Among them, Coulomb counting is one of the most commonly used methods. However, its accuracy is highly dependent on sensor accuracy and it also suffers from unknown initial error [3, 4]. As it is an open loop estimator, the accumulated error causes a drift and results in poor estimation accuracy. Open circuit voltage (OCV) method is another commonly used method. However, it needs the battery to be rested for a long period to estimate the battery's OCV [5]. As such, it is not practical for applications such as satellite whereby the battery is being used all the time. Hybrid method using the Coulomb counting and battery voltage has been used to overcome the shortfalls of Coulomb counting and OCV methods. One such example is using charging and discharging end voltages [6, 7]. However, these voltages are highly dependent on the current and operating temperature. The needs of full charge and discharge cycles shorten the battery lifespan which is not desirable for many applications. Battery impedance has been used to estimate SOC as well but it is more suitable for offline purposes [8, 9].

Model-based SOC estimators using extended Kalman filter (EKF) [10–14], H_∞ [15, 16] and observer-based [17–19] methods have become more common in recent years. The EKF method requires the linearisation process of Jacobian matrix derivation and its derivation is not trivial [1]. Computational intelligence methods such as artificial neural networks have been used in SOC and state of health (SOH) estimation [20–23]. Their accuracy depends on the quality of the training data sets and the computational requirement is high. In previous methods, the SOC estimations are performed at room temperature [7, 12, 17] and using constant battery parameters [12, 19]. In practice, the battery parameters are affected by many factors such as SOC and ambient temperatures. In satellite application, the temperature varies at different orbital time and it has a significant effect on battery parameters and SOC.

In this paper, a dual square root unscented Kalman filter using unit spherical unscented transform (DUKFST) is proposed to estimate SOC and update the battery parameters for a VELOX-I nanosatellite from Satellite Research Center of Nanyang Technological University. The unscented Kalman filter takes advantage of deterministic sampling method with a higher accuracy of second order than the first order EKF in estimating the mean and covariance of the state vector [12]. It avoids the derivation of Jacobian matrix to linearise a non-linear process, which is one of the major drawbacks of EKF. With spherical unscented transform, it uses fewer sigma points than the typical unscented transform and requires only one weighted tuning parameter instead of three parameters required by the regular UKF [12, 13]. The square root aspect of the filter improves the numerical stability by ensuring the state covariance is always semi-positive definite [24]. However, all the Kalman filter based methods require the knowledge of process and measurement noise which could affect filter convergence and performance if not determined properly [12]. The noise covariance of the Kalman filter has been adaptively updated through the scaling factor using covariance matching in this paper. The proposed method has been verified experimentally using the nanosatellite payload profile and benchmarked with unscented Kalman filter based on unit spherical unscented transform (UKFST) and EKF methods. It is shown that the proposed method has a better performance in terms of lower root mean square error (RMSE) across different temperatures at 0,

25 and 50°C. The three temperatures are selected based on the internal satellite operating temperature range in the orbit.

The outline of this paper is as follows. In Section 2, the lithium ion battery model and its state space system are presented. Section 3 presents the proposed DUKFST for SOC estimation and the updating of battery parameters. Section 4 presents the experimental setup and results of the proposed method. Section 5 concludes this paper.

2 Lithium-ion battery model

Different circuit models have been used to describe the internal dynamics of a battery. Commonly used approaches include one RC network [25, 26] and two RC networks [27, 28]. Multiple branches of RC networks can be added depending on the required accuracy and the computational complexities [29, 30]. Double polarisation model using the two RC networks as shown in Fig. 1 is used in this paper [27, 28].

In Fig. 1, V_{OC} represents the battery OCV and it is a function of battery SOC and temperature (T). I_B is the battery current and V_t is the battery terminal voltage. I_B, V_t and T are the available measurements for monitoring of battery in a battery management system. R_O represents the instantaneous voltage drop to model the resistance from electrolyte and RC networks are used to represent the relaxation effects of the battery during the charging and discharging process. The battery parameters are affected by ambient temperatures, SOC, current and ageing factors. Among them, the ambient temperature is one of the main factors that affects battery parameters [31]. In this study, Li-ion (NCR18650) battery with a nominal capacity of 2.9 Ah is used. It has a maximum charge voltage of 4.2 V and a discharge voltage of 2.5 V. Fig. 2*a* shows the experimental battery response at different temperatures when a 1.45 A discharge pulse with 10 s duration is applied on the battery. The detail of the experimental setup is explained later in Section 4. Fig. 2*b* illustrates the performance of battery having different released capacity at different temperatures when the battery is discharged from the fully charged state to the fully discharged state by a constant 1.45 A discharge current. From Fig. 2, it is observed that the internal dynamic response of the battery varies at different temperatures. As such, online identification and updating of battery parameters are necessary to improve the battery model accuracy if it is expected to operate at different temperatures.

2.1 OCV against SOC at 0, 25 and 50°C

It is well-known that the V_{OC} and SOC have a non-linear relationship. The V_{OC} is also affected by ambient temperature as shown in Fig. 3. To illustrate the temperature effect on V_{OC}, the battery ambient temperature is varied from 25 to 0°C (cold temperature) and 25 to 50°C (hot temperature). Fig. 3 shows how the battery V_{OC} changes at different (hot and cold) temperatures.

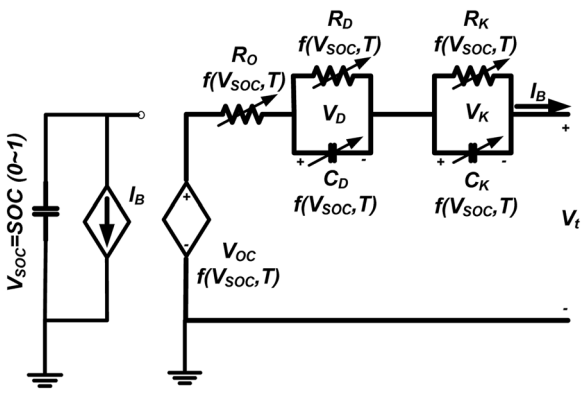

Fig. 1 *Temperature dependent double polarisation model*

In Fig. 3*a*, it is observed that V_{OC} of the battery with a 50% SOC dropped to a lower value when the temperature is decreased from 25 to 0°C. Moreover, the V_{OC} moves back to the original value when the temperature rises back to 25°C. Fig. 3*b* shows the case that the temperature is increased from 25 to 50°C.

To study the relationship between V_{OC} and SOC, the open circuit test is performed [12, 32]. In this study, the hysteresis effect of battery is neglected. The hysteresis can be included if an additional voltage source is connected in parallel with V_{OC} in Fig. 1 with increased complexity [33–35]. For this experiment, the battery is first fully charged using constant current and constant voltage (CC-CV) method. It is then rested for an hour to allow V_t to reach the equilibrium voltage and V_t is recorded as V_{OC}. The battery is subsequently discharged at 10% SOC level interval by constant discharge current of 0.58 A followed by 1 hour rest period before V_{OC} is measured. The experiment is repeated until the battery is fully discharged. V_{OC} at different temperatures (0 and 50°C) are subsequently conducted in the same manner using a thermal chamber. Fig. 4 shows the V_{OC} and SOC relationship at 0, 25 and 50°C. In Fig. 4, the V_{OC} at the fully discharged stage is around 3.2 V and is different from the maximum discharge voltage of 2.5 V. The 2.5 V is the maximum discharge voltage and the V_{OC} is obtained after resting the battery for an hour after it is discharged till the maximum discharge voltage. Similar characteristics in terms of voltage difference between the discharge curve and the OCV-SOC relationship can also be found in [32].

Using Fig. 4, the relationship of V_{OC} and SOC (ζ) can be described by a 7th order polynomial using a polynomial curve-fitting method

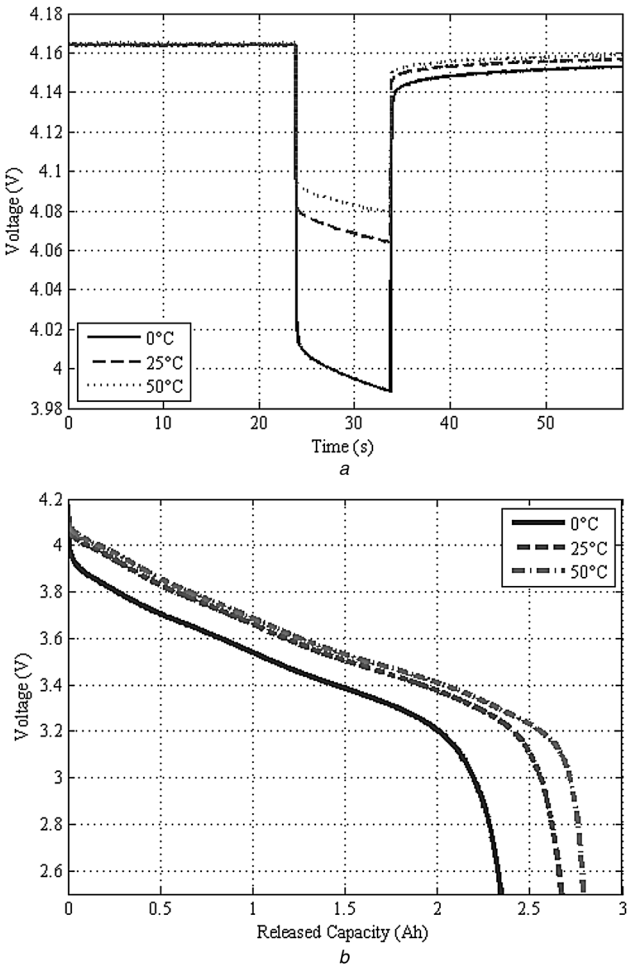

Fig. 2 *Experimental battery response at different temperatures* Q2

a 1.45 A (0.5 C) 10 s discharge pulse response at 100% SOC
b 1.45 A constant current discharge curves at different temperatures (0, 25 and 50°C)

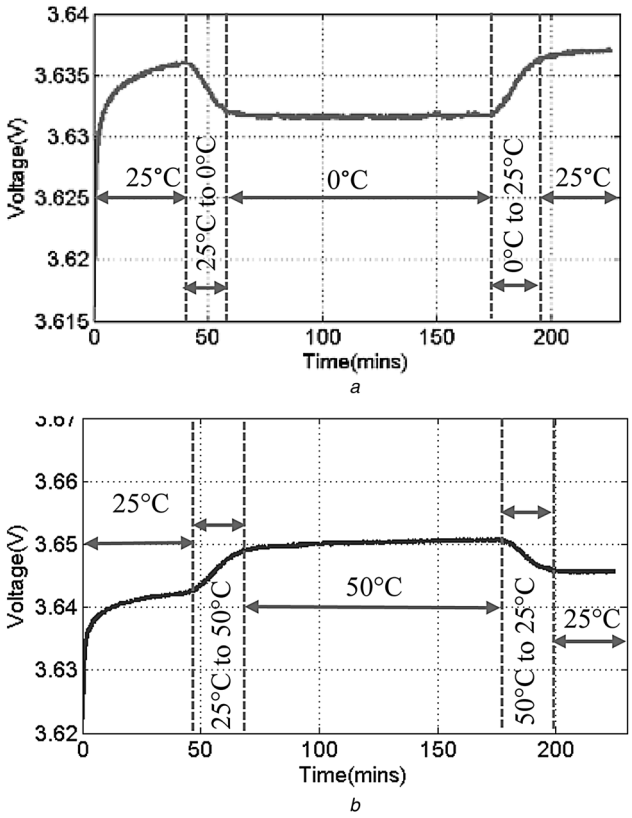

Fig. 3 *Response of V_{OC} at 50% SOC when temperature changes from*
a 25 to 0°C
b 25 to 50°C

as follows

$$V_{\mathrm{OC}}(\zeta, T) = m_1\zeta^7 + m_2\zeta^6 + \ldots + m_6\zeta^2 + m_7\zeta + m_8 \quad (1)$$

where the coefficients are $m_1 = -20.553$, $m_2 = 80.694$, $m_3 = -120.81$, $m_4 = 83.352$, $m_5 = -22.502$, $m_6 = -1.542$, $m_7 = 2.418$ and $m_8 = 3.124$ for the case of 25°C.

2.2 Modelling of battery

Let ζ be the battery SOC, V_D and V_K be the voltages across the two RC networks in Fig. 1. The dynamics of the voltage across the two RC networks (V_D and V_K) and SOC are given by [12–14]

$$\begin{aligned}\dot{\zeta}(\dot{V}_{\mathrm{SOC}}) &= -\frac{I_{\mathrm{B}}}{Q_{\mathrm{b}}}\\ \dot{V}_D &= -\frac{V_D}{R_D(\zeta, T)C_D(\zeta, T)} + \frac{I_{\mathrm{B}}}{C_D(\zeta, T)}\\ \dot{V}_K &= -\frac{V_K}{R_K(\zeta, T)C_K(\zeta, T)} + \frac{I_{\mathrm{B}}}{C_K(\zeta, T)}\end{aligned} \quad (2)$$

where Q_{b} represents the battery nominal capacity from the battery datasheet after ignoring the temperature and cycle dependencies [17, 25] and T is the battery temperature. The battery internal state variables, x, is defined as $x = \begin{bmatrix}\hat{\zeta}_{k+1} & \hat{V}_{D_{k+1}} & \hat{V}_{K_{k+1}}\end{bmatrix}^{\mathrm{T}}$. Using Fig. 1 and (2), the battery state process function, F and measurement function, H, can then be derived as [12–14]

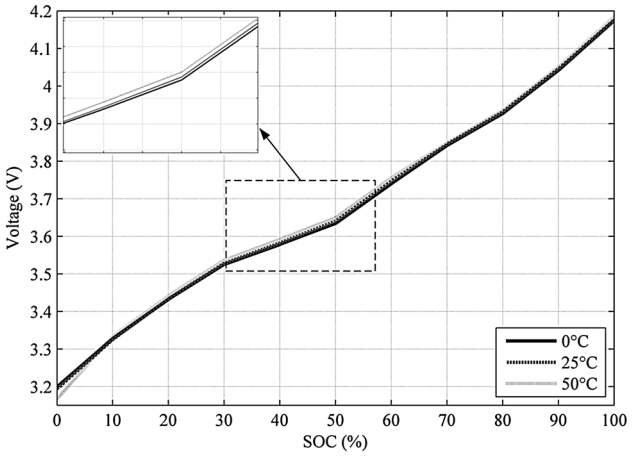

Fig. 4 *V_{OC} against SOC at 0, 25 and 50°C*

$$\begin{aligned}F(\zeta, V_D, V_K, T) &= \begin{bmatrix}\zeta_{k+1}\\ V_{D_{k+1}}\\ V_{K_{k+1}}\end{bmatrix} = \begin{bmatrix}1 & 0 & 0\\ 0 & \mathrm{e}^{-\Delta t/R_DC_D} & 0\\ 0 & 0 & \mathrm{e}^{-\Delta t/R_KC_K}\end{bmatrix}\begin{bmatrix}\zeta_k\\ V_{D_k}\\ V_{K_k}\end{bmatrix}\\ &\quad + \begin{bmatrix}-\dfrac{\Delta t}{Q_{\mathrm{b}}}\\ R_D(1-\mathrm{e}^{-\Delta t/R_DC_D})\\ R_K(1-\mathrm{e}^{-\Delta t/R_KC_K})\end{bmatrix}[I_{\mathrm{B}}]\\ \hat{V}_{\mathrm{t}} &= H(x, z, I_{\mathrm{B}}, T) = \hat{V}_{\mathrm{OC}}(f(V_{\mathrm{SOC}}, T)) - \hat{V}_D(V_{\mathrm{SOC}}, T)\\ &\quad - \hat{V}_K(V_{\mathrm{SOC}}, T) - I_{\mathrm{B}}\hat{R}_O(V_{\mathrm{SOC}}, T)\end{aligned} \quad (3)$$

where Δt represents the sampling time and I_{B} and V_{t} are the battery current and terminal voltage measurements. Let the battery parameters be defined as $z = \begin{bmatrix}\hat{R}_O & \hat{R}_D & \dfrac{1}{\hat{C}_D} & \hat{R}_K & \dfrac{1}{\hat{C}_K}\end{bmatrix}^T$. Battery parameters need to be identified to estimate battery state variables. To extract the battery parameters, various charge and discharge pulses are injected into the battery at different SOC intervals. Within the short observation time window, the battery system can be considered as time invariant system and the transfer function method can be used to identify the battery parameters [12]. To obtain the transfer function, Laplace transform is carried out on (2). The V_{t} in frequency domain is then written as

$$V_{\mathrm{t}}(s) = V_{\mathrm{OC}}(s) - I_{\mathrm{B}}(s)R_O - \frac{R_DI_{\mathrm{B}}(s)}{1 + R_DC_Ds} - \frac{R_KI_{\mathrm{B}}(s)}{1 + R_KC_Ks} \quad (4)$$

By considering V_{t}–V_{OC} as output and the current I_{B} as the input, the transfer function $G(s)$ can be obtained as (see (5))

To extract the battery parameters, various charge and discharge pulses are injected into the battery at different SOC intervals and the corresponding voltage responses are measured. Using the voltage responses and the corresponding injected current pulses, the transfer function coefficients (a_2, a_1, a_0, b_1 and b_0) of $G(s)$ can be obtained. The battery parameters (R_O, R_D, C_D, R_K and C_K) can then be obtained by solving the transfer function coefficients. Different set of transfer functions and parameters are identified

$$G(s) = \frac{V_{\mathrm{t}}(s) - V_{\mathrm{OC}}(s)}{I_{\mathrm{B}}(s)} = -\frac{a_2s^2 + a_1s + a_0}{s^2 + b_1s + b_0} = -\frac{R_Os^2 + ((R_O/R_DC_D) + (R_O/R_KC_K) + (1/C_D) + (1/C_K))s + ((R_O + R_1 + R_2)/R_DC_DR_KC_K)}{s^2 + ((1/R_DC_D) + (1/R_KC_K))s + (1/R_DC_DR_KC_K)} \quad (5)$$

Table 1 Identified initial battery parameters

R_O	54.28 mΩ
R_D	10.58 mΩ
R_K	40.16 mΩ
C_D	330 F
C_K	1020 F

with respect to each measure voltage at each SOC level. Then, the average of all identified parameters is taken as the initial battery parameters. The detail process to extract the initial battery parameters can be found in [12]. The identified initial battery parameters are shown in Table 1.

However, these battery parameters vary at different temperature and SOC. They are updated through spherical square root unscented Kalman filter, which will be explained in the next section, to improve the battery model accuracy across different SOC and ambient temperature.

3 Dual spherical square-root unscented Kalman filter-based SOC estimation

Model-based estimation using EKF has been extensively used in SOC and SOH estimation. However, there are a few drawbacks in the EKF. One of the drawbacks is the need to linearise state functions as part of the calculation of Jacobian matrices. This could lead to divergence and instability of the filter. When the state transition and measurement functions are highly non-linear, EKF could give a poor performance. To overcome the drawbacks, UKF uses a deterministic sampling approach. Using unscented transform, a minimal set of points called sigma points are used to propagate the state mean and covariance. These points are propagated through the non-linear functions thus avoiding the need to linearise the functions. There are different types of unscented transforms for sigma points selection. In this paper, the spherical transform is proposed which has the advantages of fewer sigma points and tuning parameters than the regular unscented transform [36].

In standard UKF, the state covariance $\boldsymbol{P}_k$ is recursively updated and propagated by decomposing into matrix square-root $S_k$for sigma point mapping at each time step where $\boldsymbol{P}_k = S_k S_k^T$. $\boldsymbol{P}_k$ matrix is then reconstructed from all propagated sigma points for updating purpose. On the other hand, the Sqrt-UKFST directly propagates and updates S_k without the need of decomposing and reconstructing matrix $\boldsymbol{P}_k$. This avoids the need of refactorisation on $\boldsymbol{P}_k$ at each time step. Thus positive semi-definiteness of the $\boldsymbol{P}_k$ could be guaranteed which results in improved numerical stability [24]. The square root UKF makes use of three linear algebra techniques for square-root covariance updates and propagation: QR decomposition (*qr*), Cholesky factor updating (*cholupdate*) and efficient least squares.

Given a n-dimensional state space model of a non-linear system and output equations as follows

$$\begin{aligned} \hat{x}_{k+1} &= f(\hat{x}_k, u_k) + \gamma_k w_k \\ \hat{y}_k &= h(\hat{x}_k, u_k) + v_k \end{aligned} \tag{6}$$

where u_k is the system input variables, x_k is the system state variables and y_k is the state output variables. The state-space and the measurement models are $f(x, u)$ and $h(x, u)$, respectively. Let $Q_k \sim N(0, cov_Q)$ and $R_k \sim N(0, cov_R)$ represent the Gaussian process and measurement noises, respectively. Through the spherical transform, the n state variables can be transformed into $n+2$ sigma points χ_i with the weight w_i. The approach to select weights (w_i) and sigma points (χ_i) is presented in [36]. The sigma points are propagated through the state function $f(x_k, u_k)$ and these propagated sigma points are used to estimate the system output $\tilde{y}$ using $h(x_k, u_k)$ in (5). The Kalman filter gain K is calculated through S_k and the cross covariance P_{xy}. Then the state mean and covariance are updated using the computed Kalman gain, K.

The error covariance of Q and R can affect the filter performance. To further improve the filter performance, different adaptive filtering methods: maximum likelihood, Bayesian estimation and covariance matching have been used to adaptively update Q and R [37]. One of the adaptive Kalman filtering techniques is covariance matching which makes the elements of the innovation or residual-based covariance matrix consistent with the theoretical values. The estimated covariance matrix of the innovations or residuals should match with its theoretical form. Based on this assumption, the philosophy of estimating Q and R matrices takes place

$$\begin{aligned} v_k &= y_k - H_k \bar{x}_k \\ E\{v_k v_k^T\} &= H_k \hat{P}_k^- H_k^T + R_k \\ C_v^{k,N} &= \frac{1}{N} \sum_{j=k-N+1}^{k} v_j v_j^T \end{aligned} \tag{7}$$

However, the simultaneous adaptation of both Q_k and R_k is not considered robust as discussed in [38, 39]. It is the state process noise, which is unknown. Based on this assumption, Q_k can be adapted using the adaptive factor, α [40, 41].

$$\begin{aligned} \alpha &= \frac{\text{trace}\{\hat{C}_v - R_k\}}{\text{trace}\{H_k \bar{P}_k H_k^T\}} \\ \alpha &= \frac{\text{trace}\{H_k(\Phi_{k-1}\tilde{P}_{k-1}\Phi_{k-1}^T + \hat{Q}_{k-1})H_k^T\}}{\text{trace}\{H_k(\Phi_{k-1}\hat{P}_{k-1}\Phi_{k-1}^T + Q_{k-1})H_k^T\}} \\ \hat{Q}_k &= \alpha \hat{Q}_{k-1} \end{aligned} \tag{8}$$

With the adaptive process noise, dual estimation with two separate Kalman filters can be used for state and parameters estimation [10, 11, 24]. The summary of DUKFST is summarised in Table 2.

4 Experimental setup and analysis

To validate the proposed method, a battery test bench as shown in Fig. 5 has been set up. It consists of a power supply (Agilent E3631A) to simulate the charging from solar power, a DC electronic load (Prodigit 3311F) to simulate the loading effects of satellite subsystems and a thermal chamber (SE-300) for temperature control. The thermal chamber is used to maintain at different temperatures to simulate the different operating range of the battery at different orbits. The temperatures used for the experiment are at 0, 25 and 50°C following the satellite expected temperature operation range. The experimental results were collected with a data acquisition board (NI PXI-1036) via a general purpose interface bus communication for reference SOC estimation. The reference SOC is obtained using the calibrated ampere hour counting via the high precision current sensors from the power supply and the DC electronics load with the sensor accuracy of 0.2 and 0.1%, respectively. All the hardware equipment are controlled by LABVIEW software.

The setup is then used to perform VELOX-I nanosatellite payload mission experiment as shown in Fig. 6 to validate the proposed method. There are two different loading profiles for the nanosatellite: normal operation and payload operation. For the normal operation, the load profile does not have many dynamic load change. The VELOX-I payload operation dynamic loading pattern is similar to the urban dynamometer driving schedule which is used as the standard benchmark load profile in battery testing [9, 11].

4.1 Robustness and convergence analysis in terms of initial SOC error

The proposed method is first verified for its robustness in terms of initial SOC error. Assuming that there is an error in the initial

Table 2 Summary of DUKFST

Step1: Set the initial state $\hat{x}_o = [\,\hat{\zeta} \quad \hat{V}_D \quad \hat{V}_K\,]^T$, parameter $\hat{z}_o = \left[\,\hat{R}_O \quad \hat{R}_D \quad \frac{1}{\hat{C}_D} \quad \hat{R}_K \quad \frac{1}{\hat{C}_K}\,\right]^T$ and covariance S_x and S_z:

$$\hat{x}_0 = E[x_0], \quad S_{x_0} = \text{chol}\left\{E[(x_0 - \hat{x}_0)(x_0 - \hat{x}_0)^T]\right\}$$

$$\hat{z}_0 = E[z_0], \quad S_{z_0} = \text{chol}\left\{E[(z_0 - \hat{z}_0)(z_0 - \hat{z}_0)^T]\right\}$$

Step 2: Compute the sigma points χ_i,

$$\chi_{i,k-1} = \hat{x}_{k-1} + S_{x,k-1}\chi_i^n, \quad i = 0, 1, \ldots, n+1$$

Step 3: State estimates propagation,

$$\chi_{k|k-1} = F(\chi_{k-1}, I_{B,k-1})$$

$$\hat{x}_k^- = [\,\hat{\zeta}_k^- \quad \hat{V}_D^- \quad \hat{V}_K^-\,]^T = \sum_{i=0}^{n+1} W_{x,i}\chi_{k|k-1}$$

$$S_{x,k}^- = qr\left\{\left[\,\sqrt{W_{x,i}}(\chi_{1:n+1,k|k-1} - \hat{x}_k^-) \quad \sqrt{Q_x}\,\right]\right\}$$

$$S_{x,k}^- = \text{cholupdate}\{S_{x,k}^-, \chi_{0,k|k-1} - \hat{x}_k^-, W_{x,0}\}$$

Step 4: Calculation of estimated measurement Υ_k and mean $\hat{y}_k^-$

$$\Upsilon_{k|k-1} = H[\chi_{k|k-1}, I_{B,k-1}] \quad \hat{y}_k^- = \hat{V}_t^- = \sum_{i=0}^{n+1} W_{x,i}\Upsilon_{i,k|k-1}$$

Step 5: Compute the measurement covariance $S_{\hat{y}_k}$ and its update

$$S_{\hat{y}_k} = qr\{[\,\sqrt{W_{x,i}}(\Upsilon_{1:n+1,k|k-1} - \hat{y}_k^-) \quad \sqrt{R}\,]\}$$

$$S_{\hat{y}_k} = \text{cholupdate}\{S_{\hat{y}_k}, \Upsilon_{0,k|k-1} - \hat{y}_k^-, W_{x,0}\}$$

Step 6: Calculation of cross covariance matrix $P_{x_k y_k}$

$$P_{x_k y_k} = \sum_{i=0}^{n+1} W_{x,i}(x_{i,k|k-1}^+ - \hat{x}_k^-)(\Upsilon_{i,k|k-1} - \hat{V}_{t,k}^-)^T$$

Step 7: Calculation of Kalman gain K_x and state estimate update $\hat{x}_k^+$ through measurement V_t

$$K_{x,k} = P_{x_k y_k} S_{\hat{y}_k}^{T^{-1}} S_{\hat{y}_k}^{-1} \quad \hat{x}_k^+ = \hat{x}_k^- + K_{x,k}(V_{t,k} - \hat{V}_{t,k}^-)$$

Step 8: Covariance matrix update

$$U_x = K_{x,k} S_{\hat{y}_k}$$

$$S_{x,k} = \text{cholupdate}\{S_{x,k}^-, U_x, -1\}$$

Step 9: Time update and sigma-points calculation (parameter)

$$\hat{z}_k^- = \hat{z}_{k-1}$$

$$S_{z_k}^- = \lambda_{\text{RLS}}^{-1/2} S_{z_{k-1}}$$

$$z_{i,k-1} = \hat{z}_{k-1} + S_{z_{k-1}} Z_i^n, \quad i = 0, 1, \ldots, n+1$$

$$D_{k|k-1} = H(x_k, z_{k-1}, I_{B,k-1})$$

$$\hat{d}_k = \sum_{i=0}^{n+1} W_{z,i} D_{i,k|k-1}$$

$$S_{d_k} = qr\left\{\left[\,\sqrt{W_{z,i}}(Z_{1:n+1,k|k-1} - \hat{z}_k^-) \quad \sqrt{Q_z}\,\right]\right\}$$

$$S_{d_k} = \text{cholupdate}\{S_{d_k}, D_{0,k|k-1} - \hat{d}_k, W_{z,0}\}$$

Step 10: Calculation of cross covariance matrix $P_{z_k y_k}$

$$P_{z_k d_k} = \sum_{i=0}^{n+1} W_{z,i}(Z_{i,k|k-1}^+ - \hat{z}_k^-)(D_{i,k|k-1} - \hat{d}_k)^T$$

Step 11: Calculation of Kalman gain $K_{z,k}$ and parameter estimate update $\hat{z}_k^+$ through measurement ($y_k = V_t$)

$$K_z = P_{z_k d_k} S_{d_k}^{T^{-1}} S_{d_k}^{-1} \quad \hat{z}_k^+ = \hat{z}_k^- + K_z(V_{t,k} - \hat{d}_k^-)$$

Step 12: Covariance matrix update

$$U_z = K_z S_{d_k}$$

$$S_{z_k} = \text{cholupdate}\{S_{z_k}^-, U_z, -1\}$$

First, the initial covariance and state estimates are selected. Then, *Steps* 2 to 12 are recursively processed until end of the experiment (or input data).

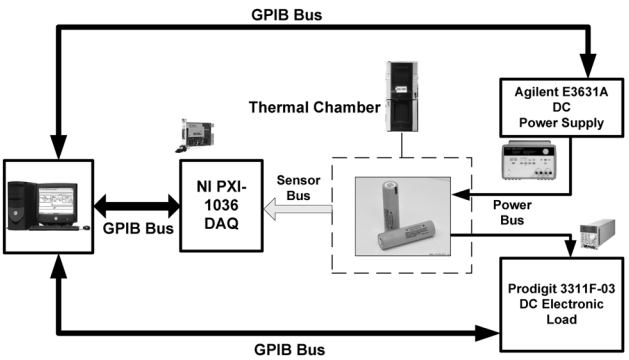

Fig. 5 *Block diagram of battery test bench*

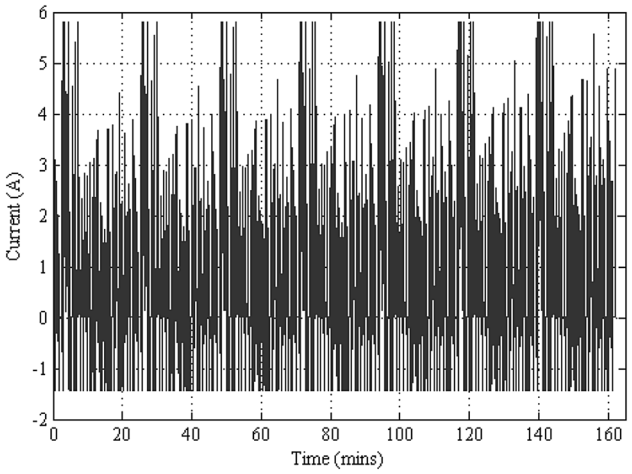

Fig. 6 *VELOX-I nanosatellite payload current profile*

SOC, the SOC estimation is performed with the load profile as shown in Fig. 6. The battery is first fully charged using CC-CV method. Owing to the high initial charging current (1.45 A) of the load profile, the battery charging voltage exceeds the absolute limit of 4.2 V. To safeguard the charged safety limit voltage when using the load profile, the battery is discharged to 80% SOC by a

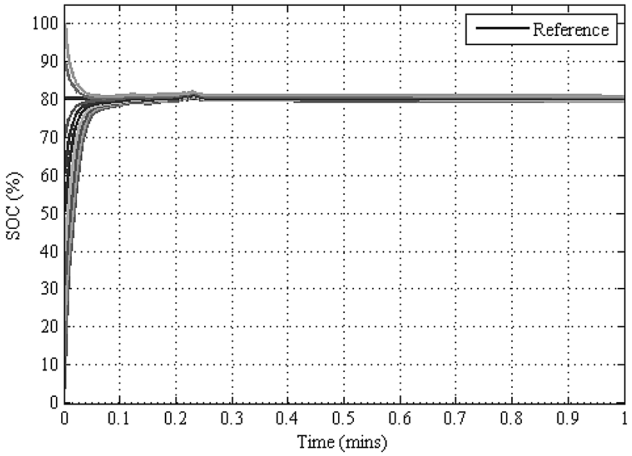

Fig. 7 *Initial SOC error analysis of 80% reference SOC at 25°C*

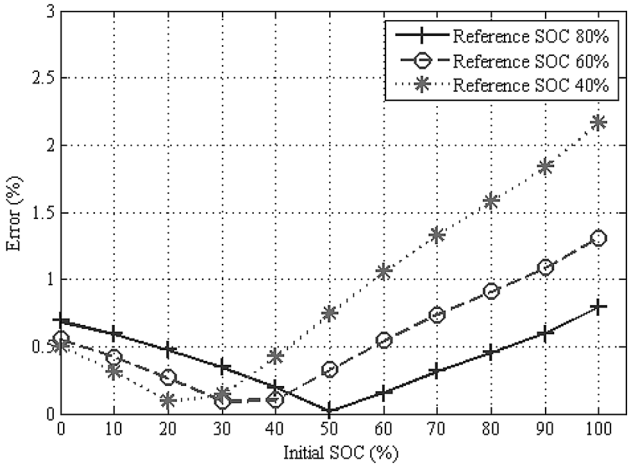

Fig. 8 *SOC estimation error under unknown initial SOC at 25°C*

Table 3 Initial SOC error analysis at 0 and 50°C

		Reference SOC					
		80%		60%		40%	
initial SOC, %	100	0.57	0.37	4.12	4.47	0.31	0.64
	90	0.38	0.08	3.92	4.14	0.05	1.1
	80	0.24	0.13	3.76	3.89	0.31	1.48
	70	0.11	0.35	3.61	3.67	0.58	1.79
	60	0.06	0.58	3.44	3.43	0.88	2.1
	50	0.22	0.78	3.25	2.22	1.21	2.39
	40	0.40	0.92	3.05	3.04	1.56	2.64
	30	0.55	1.05	2.87	2.89	1.87	2.86
	20	0.67	1.2	2.72	2.71	2.13	3.09
	10	0.79	1.38	2.58	2.51	2.36	3.37
	0	0.88	1.56	2.46	2.28	2.57	3.67
		0°C	50°C	0°C	50°C	0°C	50°C
				temperature			

discharge current of 0.29 A (0.1 C). Different initial SOC errors in terms of 10% SOC intervals from 0 to 100% are considered for the proposed method at three different temperatures: 0, 25 and 50°C. Fig. 7 shows the convergence of initial error analysis at 25°C when the reference SOC is 80%. It can be observed that the proposed method converges to the actual SOC within 20 s. To further validate the convergence performance of the proposed method, different reference SOCs, that is, 40, 60 and 80%, are performed at 0, 25 and 50°C. From Fig. 8, the DUKFST is able to converge to the reference SOC across the entire operation range with the maximum estimation error of 2.4% at 25°C. Table 3 summarises the performance at 0 and 50°C. The results show that the initial estimation error does not impact the convergence of the SOC estimation using the proposed DUKFST.

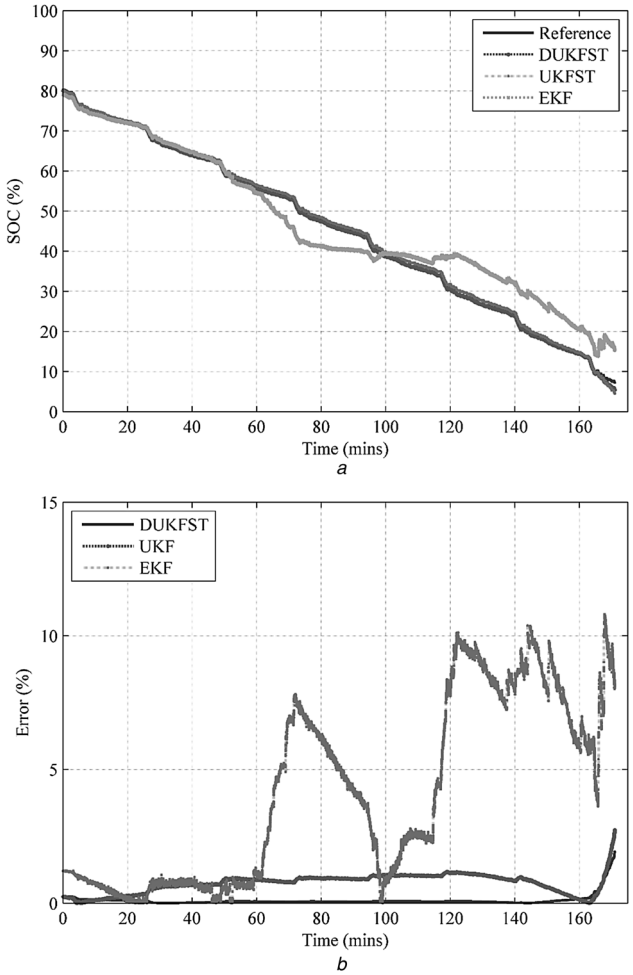

Fig. 9 *SOC*

a Estimation
b Absolute error comparison against reference SOC by DUKFST, UKFST and EKF at 50°C

4.2 SOC Estimation at 0, 25 and 50°C

For a given initial SOC and battery parameters in Table 1, SOC estimation is performed using the load profile in Fig. 6 at three different temperatures: 0, 25 and 50°C. The performance of the proposed method is then compared against UKFST and EKF. For performance evaluation, the following RMSE and absolute maximum errors are used

$$\text{RMSE} = \sqrt{\frac{1}{n}\sum_{k=1}^{n}\left(\zeta_k - \hat{\zeta}_k\right)^2} \qquad (9)$$

$$\text{Maximum} = \text{Max}\left|\zeta_k - \hat{\zeta}_k\right|$$

Fig. 9 presents the SOC estimation comparison with the reference SOC and its absolute error between the estimated and reference SOC from DUKFST, UKFST and EKF at 50°C. From Fig. 9, it can be observed that DUKFST and UKFST follow more closely to the reference SOC than the EKF. Fig. 9*b* shows that DUKFST produces the least estimation error.

Using the same load profile, the experiment is conducted at 0 and 25°C. Fig. 10 shows the corresponding absolute SOC estimation error, respectively. From Fig. 10, it can be seen that the proposed method outperforms the UKFST and EKF especially at 0 and 50°C.

The improvement in performance is because of the updating of battery parameters by the proposed method. Fig. 11 shows the values of R_O, τ_D and τ_K at 0, 25 and 50°C. These estimated values during the experiment are plotted against SOC to have a clearer

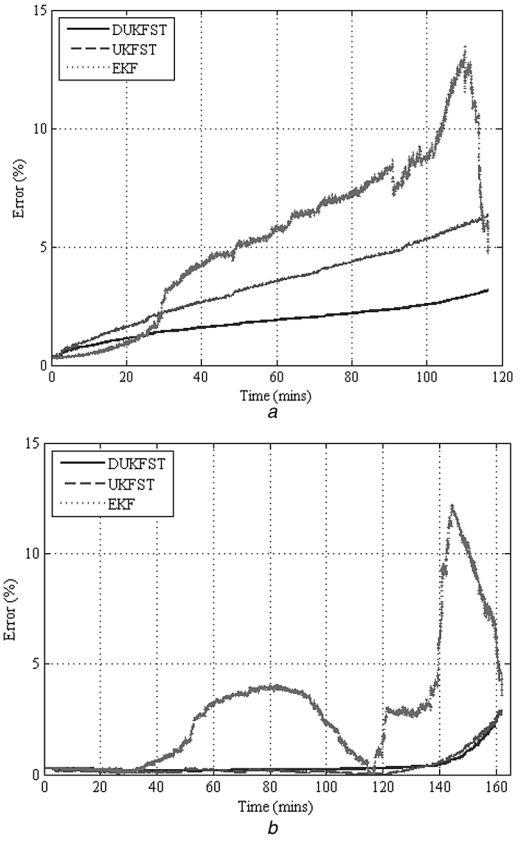

Fig. 10 *SOC estimation error comparison at*

a 0°C
b 25°C

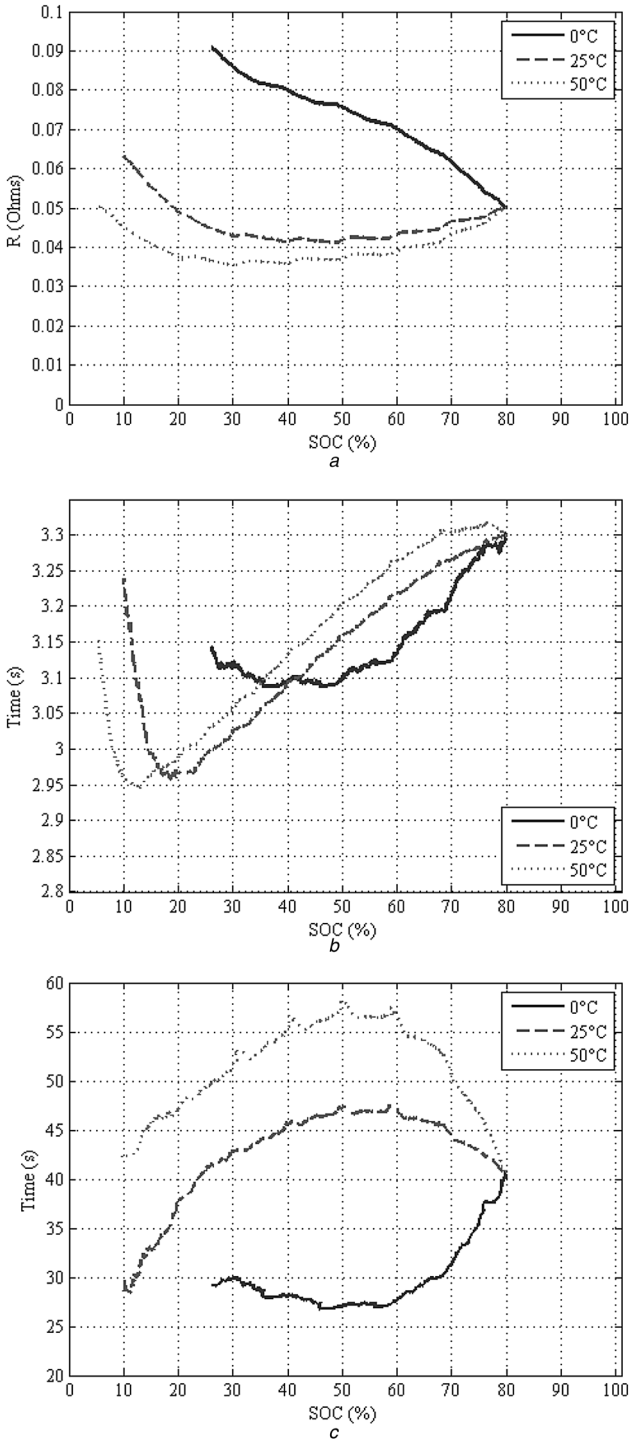

Fig. 11 *Estimated battery parameters*

a R_O
b τ_D and
c τ_K at 0, 25 and 50°C

understanding how the battery parameters changes across different SOC level and at different temperatures. It can be observed that the parameters of battery vary across different temperature and SOC. From Fig. 11*a*, R_O is higher in cold temperature and lower in hot temperature as expected. However, these updated parameters might not reflect the actual battery parameters values. Still, it is able to represent the V_t used for the SOC estimation in this paper. Table 4 shows the performance comparison between the proposed DUKFST, UKFST and EKF. From Table 4, it can be seen that DUKFST has lower RMSE and maximum error than UKFST and EKF across different temperatures.

Table 4 Performance comparison between DUKST, UKFST and EKF

		DUKFST	UKFST, %	EKF, %
0°C	RMSE	1.96%	3.78	6.3
	% increase w.r.t DUKST	–	93	221
	maximum	3.36%	6.66	13.5
	% increase w.r.t DUKST	–	98	302
25°C	RMSE	0.58%	0.62	4.1
	% increase w.r.t DUKST	–	6.9	607
	maximum	2.86%	2.9	12.2
	% increase w.r.t DUKST	–	1.4	321
50°C	RMSE	0.36%	0.83	5.3
	% increase w.r.t DUKST	–	131	1372
	maximum	1.93%	2.73	10.8
	% increase w.r.t DUKST	–	41	460

Table 5 Multiplication comparison analysis between DUKST, UKFST and EKF

	Multiplication required		
Operation	DUKFST	UKFST	EKF
P_{xx}	$(n+2)n^2$	$(n+2)n^2$	–
P_{xy}	$(n+2)(nL)$	$(n+2)(nL)$	–
P_{yy}	$(n+2)L^2$	$(n+2)L^2$	–
$PH^T(HPH^T+R)$	–	–	$L^3+2nL^2+2n^2L$
$K(y-\hat{y})$	L^3+nL^2+nL	L^3+nL^2+nL	$nL+Ln^2$
$P-KP_{yy}K$	Ln^2	Ln^2	n^2L+n^3
total multiplication required	$253(z=5, L=1)+81$ $(n=3, L=1)=334$	$81(n=3, L=1)$	$73(n=3, L=1)$

4.3 Computational requirement

Table 5 compares the number of multiplication required in each operation for the DUKST, UKFST and EKF. In Table 5, 'n', 'z' and 'L' denotes the number of states, the number of parameters and the number of measurements, respectively. From the table, it is observed that DUKFST has the most number of multiplication required as expected. For the comparison between DUKFST and UFKST, the total number of multiplication increased from 81 to 334. However this also resulted in the improved performance of 93 and 98% for RMSE and absolute maximum error, respectively, at 0°C. For comparison with EKF at 0°C, it represents 221 and 302% improvement for the RMSE and absolute maximum error, respectively.

5 Conclusion

Operating temperature of the satellite varies significantly in one orbit (about 100 minutes) which affects its battery parameters and SOC. Most of the observer based methods used fixed battery parameters obtained offline at room temperature. The SOC estimation accuracy is therefore degraded if the temperature fluctuates. In this paper, a new SOC estimation method and an online parameter updating algorithm using a DUKFST with unit spherical unscented transform is presented. It takes advantage of Jacobian free unscented Kalman filter and updates the parameters to improve the accuracy of battery model. Moreover, the spherical transform uses fewer sigma points than the normal unscented transform. The experimental results demonstrate that the proposed DUKFST outperforms the UKFST and EKF with the lowest RMSE and the lowest maximum errors. The improvement is particularly significant at 0 and 50°C. For the computational analysis, this improvement in performance comes from the increased computational requirement compared with UKFST and EKF.

6 References

1 Waag, W., Fleischer, C., Sauer, D.U.: 'Critical review of the methods for monitoring of lithium-ion batteries in electric and hybrid vehicles', *J. Power Sources*, 2014, **258**, pp. 321–339

2 Pop, V., Bergveld, H.J., Notten, P.H.L., Regtien, P.P.L.: 'State-of-the-art of battery state-of-charge determination', *Meas. Sci. Technol.*, 2005, **16**, pp. R93–R110

3 Codeca, F., Savaresi, S.M., Rizzoni, G.: 'On battery state of charge estimation: a new mixed algorithm'. Proc. IEEE Int Conf. on Control Applications, September 2008, pp. 102–107

4 Ng, K.S., Huang, Y.F., Moo, C.S., Hsieh, Y.C.: 'An enhanced coulomb counting method for estimating state-of-charge and state-of-health of lead-acid batteries'. Proc. 31st Int. Telecommunications Energy Conf. (INTELEC), October 2009, pp. 1–5

5 Huang, S.J., Huang, B.G., Pai, F.S.: 'An approach to measurements of electrical characteristics of lithium-ion battery with open-circuit voltage function', *IET Power Electron.*, 2012, **5**, pp. 1968–1975

6 Hussein, A.A.H., Batarseh, I.: 'A review of charging algorithms for nickel and lithium battery chargers', *IEEE Trans. Veh. Technol.*, 2011, **60**, pp. 830–838

7 Ng, K.S., Moo, C.-S., Chen, Y.-P., Hsieh, Y.-C.: 'Enhanced coulomb counting method for estimating state-of-charge and state-of-health of lithium-ion batteries', *Appl. Energy*, 2009, **86**, pp. 1506–1511

8 Li, R., Wu, J., Wang, H., Li, G.: 'Prediction of state of charge of Lithium-ion rechargeable battery with electrochemical impedance spectroscopy theory'. Proc. IEEE Fifth Industrial Electronics and Applications Conf. (ICIEA), June 2010, pp. 684–688

9 Coleman, M., Lee, C.K., Zhu, C., Hurley, W.G.: 'State-of-charge determination from EMF voltage estimation: using impedance, terminal voltage, and current for lead-acid and lithium-ion batteries', *IEEE Trans. Ind. Electron.*, 2007, **54**, pp. 2550–2557

10 Plett, G.L.: 'Sigma-point Kalman filtering for battery management systems of LiPB-based HEV battery packs: Part 2: Simultaneous state and parameter estimation', *J. Power Sources*, 2006, **161**, pp. 1369–1384

11 Plett, G.L.: 'Extended Kalman filtering for battery management systems of LiPB-based HEV battery packs: Part 3. State and parameter estimation', *J. Power Sources*, 2004, **134**, pp. 277–292

12 Aung, H., Low, K.S., Goh, S.T.: 'State-of-charge estimation of lithium-ion battery using square root spherical unscented Kalman filter (Sqrt-UKFST) in nanosatellite', *IEEE Trans. Power Electron.*, 2014, **PP**, pp. 1–1

13 Gholizade-Narm, H., Charkhgard, M.: 'Lithium-ion battery state of charge estimation based on square-root unscented Kalman filter', *IET Power Electron.*, 2013, **6**, pp. 1833–1841

14 Dai, H., Wei, X., Sun, Z., Wang, J., Gu, W.: 'Online cell SOC estimation of Li-ion battery packs using a dual time-scale Kalman filtering for EV applications', *Appl. Energy*, 2012, **95**, pp. 227–237

15 Zhang, F., Liu, G., Fang, L., Wang, H.: 'Estimation of battery state of charge with H_∞ observer: applied to a robot for inspecting power transmission lines', *IEEE Trans. Ind. Electron.*, 2012, **59**, pp. 1086–1095

16 Alfi, A., Charkhgard, M., Haddad Zarif, M.: 'Hybrid state of charge estimation for lithium-ion batteries: design and implementation', *IET Power Electron.*, 2014, **7**, pp. 2758–2764

17 Gholizadeh, M., Salmasi, F.R.: 'Estimation of state of charge, unknown nonlinearities, and state of health of a lithium-ion battery based on a comprehensive unobservable model', *IEEE Trans. Ind. Electron.*, 2014, **61**, pp. 1335–1344

18 Rahimi-Eichi, H., Baronti, F., Mo-Yuen, C.: 'Online adaptive parameter identification and state-of-charge coestimation for lithium-polymer battery cells', *IEEE Trans. Ind. Electron.*, 2014, **61**, pp. 2053–2061

19 Jun, X., Mi, C.C., Binggang, C., Junjun, D., Zheng, C., Siqi, L.: 'The state of charge estimation of lithium-ion batteries based on a proportional-integral observer', *IEEE Trans. Veh. Technol.*, 2014, **63**, pp. 1614–1621

20 Li, S.G., Sharkh, S.M., Walsh, F.C., Zhang, C.N.: 'Energy and battery management of a plug-in series hybrid electric vehicle using fuzzy logic', *IEEE Trans. Veh. Technol.*, 2011, **60**, pp. 3571–3585

21 Chang, W.-Y.: 'Estimation of the state of charge for a LFP battery using a hybrid method that combines a RBF neural network, an OLS algorithm and AGA', *Int. J. Electri. Power Energy Syst.*, 2013, **53**, pp. 603–611

22 Hu, J.N., Hu, J.J., Lin, H.B., *et al.*: 'State-of-charge estimation for battery management system using optimized support vector machine for regression', *J. Power Sources*, 2014, **269**, pp. 682–693

23 Bo, C., Zhifeng, B., Binggang, C.: 'State of charge estimation based on evolutionary neural network', *Energy Conver. Manage.*, 2008, **49**, pp. 2788–2794

24 Haykin, S.S.: 'Kalman filtering and neural networks' (Wiley, New York, 2001)

25 Kim, J., Cho, B.H.: 'State-of-charge estimation and state-of-health prediction of a li-ion degraded battery based on an EKF combined with a per-unit system', *IEEE Trans. Veh. Technol.*, 2011, **60**, pp. 4249–4260

26 Einhorn, M., Conte, F.V., Kral, C., Fleig, J.: 'Comparison, selection, and parameterization of electrical battery models for automotive applications', *IEEE Trans. Power Electron.*, 2013, **28**, pp. 1429–1437

27 Chen, M., Rincon-Mora, G.A.: 'Accurate electrical battery model capable of predicting runtime and I–V performance', *IEEE Trans. Energy Convers.*, 2006, **21**, pp. 504–511

28 Taesic, K., Qiao, W.: 'A hybrid battery model capable of capturing dynamic circuit characteristics and nonlinear capacity effects', *IEEE Trans. Energy Convers.*, 2011, **26**, pp. 1172–1180

29 Wang, W., Shu-Hung Chung, H., Zhang, J.: 'Near-real-time parameter estimation of an electrical battery model with multiple time constants and SOC-dependent capacitance', *IEEE Trans. Power Electron.*, 2014, **29**, pp. 5905–5920

30 Yao-Ching, H., Tin-Da, L., Ruei-Ji, C., Hong-Yu, L.: 'Electric circuit modelling for lithium-ion batteries by intermittent discharging', *IET Power Electron.*, 2014, **7**, pp. 2672–2677

31 Lam, L., Bauer, P., Kelder, E.: 'A practical circuit-based model for Li-ion battery cells in electric vehicle applications'. Proc. IEEE 33rd Int. Telecommunications Energy Conf. (INTELEC), October 2011, pp. 1–9

32 Chun, C.Y., Baek, J., Seo, G.-S., *et al.*: 'Current sensor-less state-of-charge estimation algorithm for lithium-ion batteries utilizing filtered terminal voltage', *J. Power Sources*, 2015, **273**, pp. 255–263

33 Baronti, F., Zamboni, W., Femia, N., Roncella, R., Saletti, R.: 'Experimental analysis of open-circuit voltage hysteresis in lithium-iron-phosphate batteries'. Proc. IEEE 39th Annual Conf. Industrial Electronics Society (IECON), March 2013, pp. 6728–6733

34 Jonghoon, K., Gab-Su, S., Changyoon, C., Bo-Hyung, C., Seongjun, L.: 'OCV hysteresis effect-based SOC estimation in extended Kalman filter algorithm for a LiFePO/C cell'. Proc. IEEE Int. Electric Vehicle Conf. (IEVC), March 2012, pp. 1–5

35 Baronti, F., Femia, N., Saletti, R., Visone, C., Zamboni, W.: 'Hysteresis modeling in li-ion batteries', *IEEE Trans. Magn.*, 2014, **50**, pp. 1–4

36 Julier, S.J.: 'The spherical simplex unscented transformation'. Proc. American Control Conf., June 2003, vol. 3, pp. 2430–2434

37 Mehra, R.K.: 'Approaches to adaptive filtering', *IEEE Trans. Autom. Control*, 1972, **17**, pp. 693–698

38 Blanchet, I., Frankignoul, C., Cane, M.A.: 'A comparison of adaptive Kalman filters for a tropical pacific ocean model', *Mon. Weather Rev.*, 1997, **125**, pp. 40–58

39 Vepa, R.: 'Adaptive state estimation of a PEM fuel cell', *IEEE Trans. Energy Convers.*, 2012, **27**, pp. 457–467

40 Mohamed, A.H., Schwarz, K.P.: 'Adaptive Kalman filtering for INS/GPS', *J. Geodesy*, 1999, **73**, pp. 193–203

41 Ding, W., Wang, J., Rizos, C., Kinlyside, D.: 'Improving adaptive Kalman estimation in GPS/INS integration', *J. Navig.*, 2007, **60**, pp. 517–529

PEL20140863

Author Queries

Htet Aung, Kay Soon Low

Q1 Please check and confirm the email id of the corresponding author.

Q2 Please check and confirm insertion of main caption for Fig. 2.